DOI: 10.1002/ejic.200900493

Ferromagnetic Coupling in a New Copper(II) Schiff Base Complex with Cubane Core: Structure, Magnetic Properties, DFT Study and Catalytic Activity

Santarupa Thakurta,[a] Partha Roy,[a,b] Ray J. Butcher,[c] M. Salah El Fallah,*[d] Javier Tercero,[d] Eugenio Garribba,[e] and Samiran Mitra*[a]

Keywords: Cluster compounds / Metallocluster / Copper / Ferromagnetic interaction / Density functional calculations / Oxidation / Magnetic properties / Schiff bases

A new tetranuclear complex, $[Cu_4L_4]\cdot 2H_2O$ (**1**), has been synthesized from the self-assembly of copper(II) perchlorate and the tridentate Schiff base ligand 4-chloro-2-[(*E*)-(2-hydroxyethylimino)methyl]phenol (H_2L). Single-crystal X-ray diffraction studies reveal that complex **1** consists of a Cu_4O_4 cubane core where the four copper(II) centers are linked by μ_3-alkoxo bridges. Each Cu^{II} ion assumes a distorted square-pyramidal geometry with $CuNO_4$ chromophore. Variable-temperature magnetic susceptibility data exhibit distinct ferromagnetic exchange interaction, corroborating with the geometrical parameters of the structural unit. Theoretical calculations based on DFT method have been used to quantify the strength of the Cu···Cu magnetic interactions which help to evaluate the experimental coupling constants: J_1 = +64.8, J_2 = +24.4 and J_3 = +3.0 cm^{-1}. The EPR spectroscopy also gives some insight on the ferromagnetic S = 2 ground state of **1**. In addition, detailed investigations have been carried out on the catalytic activity of the complex towards the oxidation of cycloalkanes using H_2O_2 as terminal oxidant.

Introduction

The development of cluster coordination complexes of copper(II) is now ubiquitous in material chemistry, mainly stimulated by their significant contribution to the field of molecular magnetism and relevance to the active sites of some metalloproteins. Cubanes are amazing metalloclusters that have attracted great attention during the past two decades, because of their intriguing physical properties[1–3] along with their potential to serve as biomimetic models of nitrogenases and hydrogenases.[4–6] Several cubane-like copper(II) complexes containing hydroxo- or alkoxo bridges have been extensively studied from a magneto-structural point of view.[7–11] Owing to the flexibility in the coordination geometry around copper(II) centers, these cubanes can show ferro- as well as antiferromagnetic exchange interactions depending on the Cu–O–Cu bridging angles and the varied distortions in the Cu_4O_4 core. The major aim of modern magneto-chemists is to develop a better understanding of the structural and chemical features governing the electron spin-spin interactions in these versatile geometric arrays of four copper ions. In this context, density functional theory (DFT) offers a promising tool that may be applied to rationalize the mechanism of magnetic exchange coupling by considering the topology of various magnetic orbitals.[12–15] The successful theoretical interpretation of the observed magnetic behavior by the DFT method has turned it into an emerging field of research and further investigations on new complexes are essential to establish the validity of this theory and explore its wide dimensions for the analysis of complicated single-molecule magnets (SMMs).

Another reason for interest in multinuclear copper(II) complexes is because of their important functional role in many catalytic enzymatic reactions.[16,17] In this background a special mention may be made of a poorly characterized particulate methane monooxygenase (pMMO) which is composed of a tri- or multinuclear cluster of copper that can carry out catalytic alkane hydroxylation and alkene epoxidation.[18] Model enzymatic reactions for the oxidation of hydrocarbons in nature have been mimicked with copper complexes in the presence of several oxidants and these are also found to be effective in the case of a wide range of hydrocarbons. The study of the oxidation of cyclo-

[a] Department of Chemistry, Jadavpur University, Kolkata 700032, India
Fax: +91-33-2414-6414
E-mail: smitra_2002@yahoo.com
[b] Department of Inorganic Chemistry, Indian Association for the Cultivation of Science, Jadavpur, Kolkata 700032, India
[c] Department of Chemistry, Howard University, 2400 Sixth Street NW, Washington, DC 20059, USA
[d] Departament de Química Inorgànica, Facultat de Química, Universitat de Barcelona, Martí i Franquès 1-11, 08028 Barcelona, Spain
E-mail: salah.elfallah@qi.ub.es
[e] Department of Chemistry, University of Sassari, Via Vienna 2, 07100 Sassari, Italy

hexane assumes a special position owing to the fact that its oxidized products are of immense industrial importance.[19] For example, cyclohexanol finds its main application in the manufacture of adipic acid which is again a raw material of nylon-6,6′, soaps and detergents, rubber chemicals, pesticides etc., whereas cyclohexanone is used as an industrial solvent and activator in oxidation reactions. The search for the use of multinuclear copper complexes as catalysts has been a continuing process[20] so as to score out the optimum or highest yield of one product selectively.

Pursuing our research on phenoxo/alkoxo-bridged multinuclear Schiff base complexes,[21–23] herein we report the synthesis, spectroscopic characterizations and structural aspects of a new tetrameric cubane-like copper(II) cluster $[Cu_4L_4]\cdot 2H_2O$ (**1**), derived from the NOO donor Schiff base ligand H_2L (1:1 condensation product of ethanolamine and 5-chlorosalicylaldehyde). Magnetic susceptibility measurements (2–300 K) reveal prominent ferromagnetic exchange interaction in the cubane core. Theoretical calculations based on DFT formalism allow the assignment of the different magnetic coupling constants and provide a suitable magneto-structural correlation for the complex. Besides this, complex **1** shows effective catalytic properties for the hydrogen peroxide oxidation of cyclohexane and cycloheptane to their corresponding hydroxylated and oxygenated products affording good yield and turnover number.

Results and Discussion

Fourier Transform Infrared Spectra

The Fourier transform infrared spectrum of complex **1** has been analyzed in comparison with that of the free Schiff base ligand H_2L in the region 4000–200 cm^{-1}. The strong absorption band at 1601 cm^{-1} in the spectrum of **1** can be assigned to the imine stretching frequency of the coordinated Schiff base ligand. The shift of this band towards lower frequency compared to that of the free Schiff base ligand (1640 cm^{-1}) indicates the coordination of the imine nitrogen atom to the metal center.[24,25] The phenolic ν_{Ar-O} in the free ligand exhibits a strong band at 1206 cm^{-1}, whereas in the complex this band is observed in the lower frequency region at 1179–1187 cm^{-1}, providing evidence for coordination to the metal ions through the deprotonated phenolic oxygen atoms.[26] Ligand coordination to the metal center is substantiated by prominent bands appearing at 445 cm^{-1} and 370 cm^{-1} which can be attributed to ν(Cu–N) and ν(Cu–O), respectively. Several weak peaks observed in the range 2876-3180 cm^{-1} are likely to be due to the aromatic and aliphatic C–H stretches. In addition, the IR spectrum also indicates the presence of water molecules as confirmed by the crystal structure. The broad band at 3256–3440 cm^{-1} is attributable to O–H stretching vibrations of lattice water molecules.[24]

UV/Vis Spectra

The electronic spectroscopic data resulting from four interacting copper(II) ions of complex **1** are not straightforward to interpret and here the main features of the spectra are presented on a preliminary basis. The intense band observed around 350–385 nm is clearly charge transfer in origin and can be attributed to the transition from the coordinated unsaturated ligand to the metal ion (LMCT). Again, the intense high energy bands at about 245 and 380 nm may be assigned to the intraligand $\pi\rightarrow\pi^*$ and $n\rightarrow\pi^*$ transitions, respectively. The broad low-intensity absorption band centered at 655 nm is a typical d-d band for the copper(II) ion.[27]

Crystal Structure Description

The molecular structure of $[Cu_4L_4]\cdot 2H_2O$ (**1**) is shown in Figure 1 as an ORTEP plot with atom-labeling Scheme. Complex **1** crystallizes in the orthorhombic space group *Pbcn* and consists of a tetrameric Cu_4L_4 moiety along with two lattice water molecules. Selected bond lengths and angles as well as interatomic distances are summarized in Table 1. The tridentate Schiff base H_2L which can adopt both chelating and bridging modes undergoes double deprotonation during the reaction and the dianionic form of the ligand L^{2-} coordinates to the metal center through the imine nitrogen, deprotonated phenolic and alkoxo oxygen atoms. By a self-assembly process four such [CuL] building blocks furnish the neutral tetranuclear complex **1** with a central cubane-like unit. The cubane structure is characterized by a Cu_4O_4 core where the anionic alkoxo-oxygen atoms act as μ_3-O bridges connecting three neighboring copper(II) ions. The vertices of the cube are alternatingly occupied by four copper(II) and four bridging alkoxide oxygen atoms, leading to two interlocked distorted tetrahedra of copper and oxygen atoms. The cubane is located on crystallographic twofold axis passing through the middle of Cu1–Cu1# and Cu2–Cu2# vectors. Thus the cubane is symmetric in nature containing two crystallographically independent metal ions, Cu1 and Cu2.

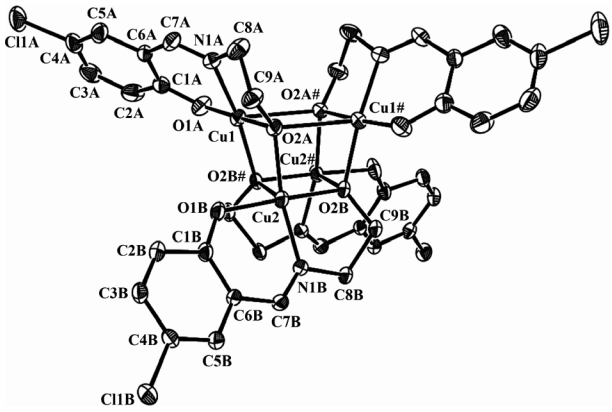

Figure 1. ORTEP representation of complex **1**. Thermal ellipsoids have been drawn at 40% probability level. Hydrogen atoms and lattice solvent molecules are omitted for clarity. Symmetry operation: # $-x$, y, $-z$ + 1/2.

Table 1. Selected bond lengths and bond angles for **1**.[a]

Bond lengths [Å]			
Cu1–O1A	1.9077(12)	Cu2–O1B	1.9055(11)
Cu1–N1A	1.9424(14)	Cu2–N1B	1.9276(12)
Cu1–O2B#	1.9507(11)	Cu2–O2A	1.9563(10)
Cu1–O2A	1.9732(11)	Cu2–O2B	1.9678(10)
Cu1–O2A#	2.4547(10)	Cu2–O2B#	2.4387(11)
Cu1···Cu2	3.06	Cu1···Cu1#	3.48
Cu1···Cu2#	3.13	Cu2···Cu2#	3.42
Bond angles [°]			
Cu2–O2A–Cu1	102.30(5)	O1A–Cu1–O2A	175.72(5)
Cu1–O2B#–Cu2	87.67(4)	O2B#–Cu1–N1A	166.75(6)
Cu1–O2B#–Cu2#	106.11(5)	O1B–Cu2–O2B	176.70(5)
Cu1–O2A#–Cu2#	89.73(4)	O2A–Cu2–N1B	169.43(5)
Cu1–O2A–Cu1#	103.12(4)	O2A–Cu1–N1A	84.64(5)
Cu2–O2B–Cu2#	101.29(4)	O1A–Cu1–N1A	91.45(6)
O2A#–Cu1–N1A	114.81(5)	O2B–Cu1–N1B	85.02(5)
O2B#–Cu2–N1B	108.74(5)	O1B–Cu2–N1B	93.64(5)

[a] Symmetry transformations used to generate equivalent atoms: # $-x$, y, $-z + 1/2$.

All copper(II) centers are pentacoordinate with a NO_4 donor set from the Schiff base ligands. For a pentacoordinate metal center, the distortion of the coordination environment from TBP to SP can be evaluated by the Addison distortion index τ, defined as $\tau = [(\beta - \gamma)/60]$, where β and γ are the two largest coordination angles around the metal[28] (τ is zero for a perfect square pyramid, while it becomes unity for an ideal trigonal bipyramidal geometry). The coordination geometry around each copper(II) center is best described as distorted square pyramidal as reflected from the respective τ values ($\tau = 0.15$ for Cu1 and Cu1#, $\tau = 0.12$ for Cu2 and Cu2#). The basal plane of the square-pyramid is constructed by the phenolate oxygen atom, the imine nitrogen atom of the salicylidene fragment, and two μ_3-alkoxide oxygen atoms while the apical position is occupied by another μ_3-alkoxide oxygen atom. Both Cu1 and Cu2 are deviated from the corresponding mean planes by 0.118 and 0.035 Å, respectively, towards the apical ligand atom. The Cu–O and Cu–N bond lengths in the equatorial plane range from 1.9055(11) to 1.9732(11) Å and from 1.9276(12) to 1.9424(14) Å, respectively (Table 1). The apical oxygen atoms show longer Cu–O bond lengths comprised between 2.4387(11) and 2.4547(10) Å, being in nice agreement with the literature values for similar systems.[1b,29] The elongation of the Cu–O axial bonds is due to a pseudo-Jahn–Teller distortion of the d^9 copper center. Each Schiff base ligand acts as a tridentate ligand for one copper(II) ion leading to five- and six-membered chelate rings with average bite angles of 84.83 and 92.54°, respectively.

In a previous paper,[30] one of the co-authors had proposed a classification of the cubane structures based on the use of the Cu···Cu distances as a classification criterion. Thus, this family of complexes are popularly divided in three classes: (i) the complexes with 2 short and 4 long Cu···Cu distances are designated as 2 + 4, (ii) those with 4 short and 2 long Cu···Cu distances are called as 4 + 2 compounds, and (iii) finally, the scarce complexes with six similar Cu···Cu distances are labeled as 6 + 0 complexes. Complex **1** clearly belongs to the 4 + 2 class with the four Cu–Cu separations including Cu1–Cu2, Cu1–Cu2# and their symmetry related counterparts Cu1#–Cu2#, Cu1#–Cu2 being significantly shorter [3.06–3.13 Å] than the Cu1–Cu1# and Cu2–Cu2# distances [3.42–3.48 Å]. The pair of Cu^{II} ions at each face of the cube is linked by double alkoxo bridges (Figure 1). The bridging Cu–O–Cu angles which determine the sign of the magnetic exchange interactions through oxygen bridges are in the range 87.67(4)°–106.11(5)°. Here, the six faces of the cube are not equivalent, the presence of two different types of planes can be recognized depending on their geometrical aspects.[10] Four $\{Cu_2O_2\}$ faces consist of two different Cu–O–Cu angles (ca. 88 and 104°) and three short Cu–O distances (ca. 1.96 Å) along with a longer one (ca. 2.45 Å). The last two $\{Cu_2O_2\}$ faces differ by the presence of a unique Cu–O–Cu angle at ca. 102° and two short (ca. 1.97 Å) and two long (ca. 2.45 Å) Cu–O distances. The distributions of the short and long Cu–O bonds in the Cu_4O_4 core are depicted in Figure 2. It is evident from the unequal Cu–O as well as Cu···Cu distances (Table 1) that the cubane core is quite distorted in shape.

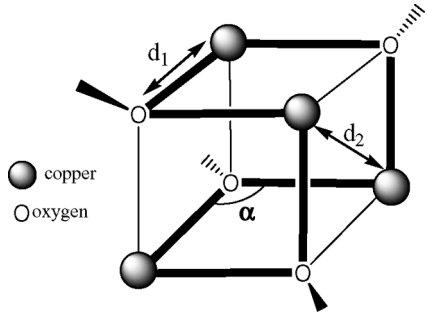

Figure 2. Structural representation of the Cu_4O_4 core showing the distribution of the short (thick lines) and long (thin lines) Cu–O bonds.

Magnetic Studies and DFT Calculations

The magnetic behavior of complex **1** is shown in Figure 3 as a $\chi_M T$ vs. T plot. At 300 K it shows a $\chi_M T$ value of 1.864 $cm^3 K mol^{-1}$ for the tetranuclear copper(II) unit, which is slightly higher than the expected value of 1.5 $cm^3 K mol^{-1}$ for four uncoupled $S = 1/2$ ions with $g = 2.0$. On cooling, $\chi_M T$ increases to reach a maximum value of 3.213 $cm^3 K mol^{-1}$ at ca. 7 K. Below this temperature $\chi_M T$ decreases to a value of 2.616 $cm^3 K mol^{-1}$ at 2 K. The shape of this curve clearly indicates dominant ferromagnetic coupling until 7 K which results from the interaction of the copper(II) ions through the alkoxo bridges. The decrease of $\chi_M T$ observed at low temperature may be attributed to the intramolecular antiferromagnetic exchange and/or the presence of the *ZFS* of the ground state $S = 2$.

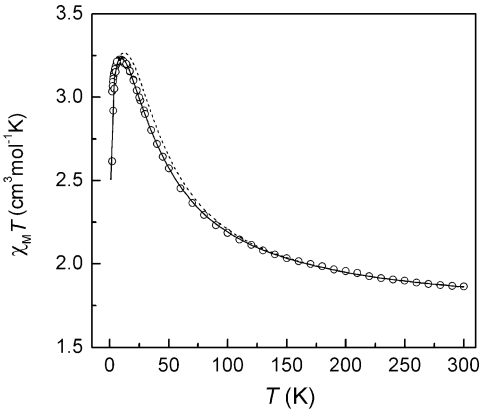

Figure 3. Temperature dependence of the $\chi_M T$ product for complex **1**. The open circles correspond to the experimental points. Solid line corresponds to the best fit curve while the dashed line corresponds to the simulated $\chi_M T$ curve using the calculated exchange coupling parameters by the B3LYP functional; g and θ values were fixed at 2.12 and –0.31, respectively (see text).

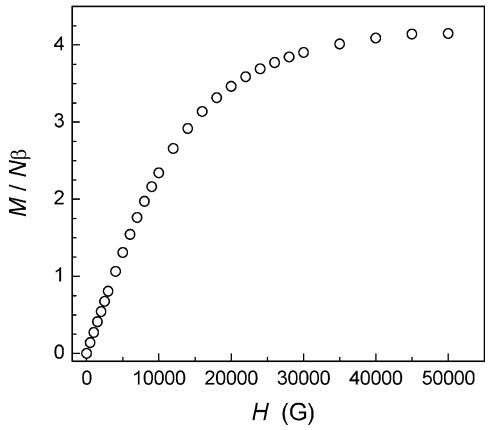

Figure 4. Plot of the field dependence of the magnetization at 2 K for complex **1**.

The field dependence of magnetization (0–5 T) measured at 2 K is shown in Figure 4 in the form of $M/N\beta$ (per Cu_4 unit) vs. H. The magnetization reaches a value of 4.15 $N\beta$ at 5 T which is close to the expected $S = 2$ value of 4 $N\beta$ for the Cu_4 system, indicating the presence of ferromagnetic interaction between the neighbouring copper(II) ions.

As discussed above, this complex may be classified as a 4+2 class of cubane having 4 short and 2 long Cu···Cu distances. Although complex **1** presents similar topology to this family, a detailed structural analysis reveals that it shows slight differences as much in Cu···Cu and Cu–O distances as in Cu–O–Cu angles (Figure 2). The main geometrical parameters influencing the exchange coupling pathways are given in Table 2.

$$\chi = 2Ng^2\beta^2 f(J,T)\, k_B(T - \theta) \quad (1)$$

where

$$f(J,T) = \frac{5\exp(E_1/2k_B) + \exp(E_2/2k_B) + \exp(E_3/2k_B) + \exp(E_4/2k_B)}{5\exp(E_1/2k_B) + 3\exp(E_2/2k_B) + 3\exp(E_3/2k_B) + 3\exp(E_4/2k_B) + \exp(E_5/2k_B) + \exp(E_6/2k_B)}$$

with

$$E_1 = J_1 + J_2 + J_3 \qquad E_2 = J_1 - J_2 - J_3 \qquad E_3 = -J_1 - J_2 + J_3 \qquad E_4 = -J_1 + J_2 - J_3$$

$$E_5 = -J_1 - J_2 - J_3 - [(2J_1 - J_2 - J_3)^2 + 3(J_2 - J_3)^2]^{(1/2)} \qquad E_6 = -J_1 - J_2 - J_3 + [(2J_1 - J_2 - J_3)^2 + 3(J_2 - J_3)^2]^{(1/2)}$$

Based on the structural features of complex **1**, we can assume three kinds of J interactions (J_1, J_2 and J_3) that group the pathways in the opposite faces of the Cu_4O_4 core (Figure 5). The analyses of the experimental susceptibility data have been performed by the use of Equation (1)[31] in conjunction with an additional Weiss constant (θ).

The E_n value can be obtained from the following Hamiltonian [Equation (2)].

$$H = -J_1(S_1 \cdot S_2 + S_3 \cdot S_4) - J_2(S_2 \cdot S_4 + S_1 \cdot S_3) - J_3(S_1 \cdot S_4 + S_2 \cdot S_3) \quad (2)$$

In the fitting process of the experimental data, we obtained different J values for J_2 and J_3 with the large errors depending of the starting parameters while the parameters J_1, g and θ converged to the values of about 64 cm^{-1}, 2.12 and –0.31, respectively.

Table 2. Main geometrical parameters and the exchange coupling constants corresponding to complex **1**.

Cu_{ij}[a]	α(Cu–O–Cu)/°	d_1(Cu–O)/Å	d_2(Cu···Cu) [Å]	J_{B3LYP}[b] [cm^{-1}]	J_{exp} [cm^{-1}]
Cu_{12}	102.3	1.956, 1.973	3.06	**+46.80(2)**	**+64.8**
Cu_{34}	102.3	1.956, 1.973	3.06		
Cu_{14}	106.1	1.951, 1.968	3.13	**+37.45(2)**	**+24.37**
Cu_{23}	106.1	1.951, 1.968	3.13		
Cu_{13}	103.1	1.973, 2.455	3.48	**+4.80(3)**	**+3.0**
Cu_{24}	101.3	1.968, 2.439	3.42	**+4.59(3)**	

[a] i and j indicate the copper atom designator considerate in the exchange coupling in each cube face. [b] The number in parentheses indicates the standard deviation of the least-squares fitting, see computational details.

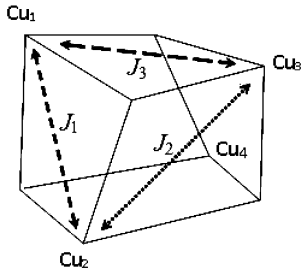

Figure 5. Different exchange coupling constants in complex **1** (Cu1, Cu2, Cu3, and Cu4 represent for Cu1, Cu2, Cu1# and Cu2#, respectively).

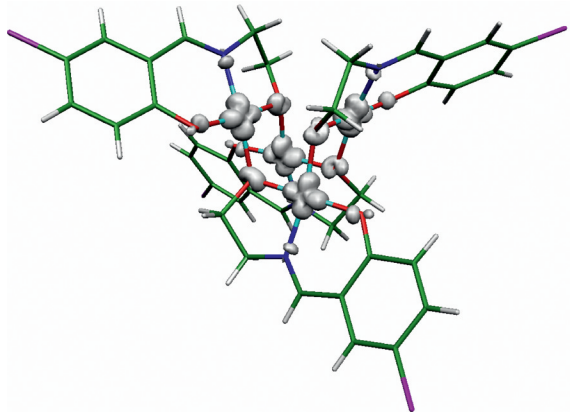

Figure 6. Spin density distribution for complex **1** corresponding to the calculated $S = 2$ ground state B3LYP solution. Positive values are represented as white surfaces.

To overcome this situation, we employ DFT (B3LYP functional) calculations by using the experimental atomic coordinates of the tetranuclear structural unit of the complex, which help us to evaluate the sign and the magnitude of the three possible exchange pathways.

The DFT calculations (for details, see DFT Methodology and Computational Details) lead to the following parameters: $J_1 = +46.80(2)$ cm^{-1}, $J_2 = +37.45(2)$ cm^{-1} and $J_3 = +4.70(3)$ cm^{-1}.

Thereafter, we use these values as starting parameters and introduce in new least square fitting of experimental data by using Equation (1), which ultimately afford the parameters: $J_1 = +64.8$ cm^{-1}, $J_2 = +24.4$ cm^{-1}, $J_3 = +3.0$ cm^{-1}, $g = 2.12$ and $\theta = -0.31$, with an error R minor than 10^{-4}, where $R = \Sigma[(\chi_M T)^2_{exp.} - (\chi_M T)^2_{cal}]/\Sigma(\chi_M T)^2_{exp.}$

In Figure 3, the theoretical $\chi_M T$ vs. T plot using the DFT calculated J values (with $g = 2.12$ and $\theta = -0.31$) is represented as a dashed line. One can appreciate the good concordance between the simulated and the experimental fitted curves.

Additionally, we also evaluate the difference in the set of the grouped J_3 values because of small differences observed in the structural data, by calculating the two possible interactions. Thus J_3 is separated in J_{3a} and J_{3b}, making easy the correlation between J values and the selected structural parameters (Table 2). The calculations give the following results: $J_1 = +46.80(2)$ cm^{-1} and $J_2 = +37.45(2)$ cm^{-1} $J_{3a} = +4.80(3)$ cm^{-1} and $J_{3b} = +4.59(3)$ cm^{-1}. Globally, it seems that the J_{ij} values obtained agree with accuracy to the reported results in the literature.[30]

The spin distribution at the paramagnetic centers is localized in the form of $d_{x^2-y^2}$ orbital. A representation of the calculated spin density for the $S = 2$ ground state can be found in Figure 6. Logically considering, the electronic configuration of the Cu^{II} cation bears the unpaired electron in M–L e_g-type antibonding orbital,[32] thereby indicating the predominance of the spin delocalization mechanism. The polarization mechanism appears to be responsible for very small negative values on some carbon atoms.

From the previously established magneto-structural correlations of such [Cu_4] cubanes, it is evident that the crucial geometrical parameters which can influence the magnetic susceptibility values are the bridging Cu–O–Cu angles and the out-of-plane shift of the atom coordinated to the bridging oxygen.[9a,15] Moreover in the case of 4 + 2 class, the presence of long Cu–O bond lengths in all exchange pathways considerably complicates the situation. The simulation of the magnetic behavior of **1** gives two predominant ferromagnetic interactions (J_1 and J_2) and a relatively weaker one (J_3). The difference in strength between the magnetic couplings can be attributed to the presence of two long Cu–O bond lengths in the case of the J_3 interaction whilst only one for either J_1 or J_2.[10] Hence, the exchange pathway between the two copper atoms in each of the four Cu···Cu pairs (Cu_{12}, Cu_{14}, Cu_{23} and Cu_{34}) involves two short Cu–O bond lengths resulting in strong ferromagnetic exchange interactions (J_1 and J_2). Accordingly, in the respective four {Cu_2O_2} planes, the near perpendicular orientation of the $d_{x^2-y^2}$ orbitals of each copper(II) ion leads to the enhancement of the ferromagnetic contribution (Figure 6). On the other hand, both Cu_{13} and Cu_{24} systems involve exchange interaction with one short and one long Cu–O bond lengths (Table 2) and the adjacent copper $d_{x^2-y^2}$ orbitals are rather parallel to each other. All these factors are responsible for the low magnitude of the coupling constant J_3.

EPR Spectra

It is well-known that for tetranuclear Cu^{II} complexes with cubane-like structure, EPR spectra are very sensitive to the core unit.[33] The spectra recorded at room temperature (r.t.) and liquid nitrogen (LN) temperature on polycrystalline complex **1** (Figure 7) are characterized by an almost isotropic and broad resonance centered at $g = 2.150$ (r.t.) and 2.100 (LN). These broad signals are indicative for a bulk concentration of copper ions having ferromagnetic interaction and a rapid intramolecular spin-spin relaxation.[34,35] The spectrum at LN temperature is better resolved and shows the features due to the hyperfine coupling between the electron and the Cu nuclei (Figure 7, a). These signals could belong to mononuclear impurities contained in the solid-state complex, as already observed for some reported tetranuclear Cu^{II} cubanes formed by Schiff bases.[36]

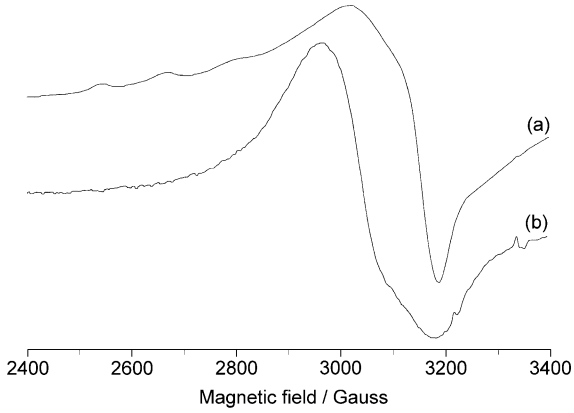

Figure 7. X-band EPR spectra recorded on the polycrystalline powder of complex **1**: (a) LN temperature and (b) r.t.

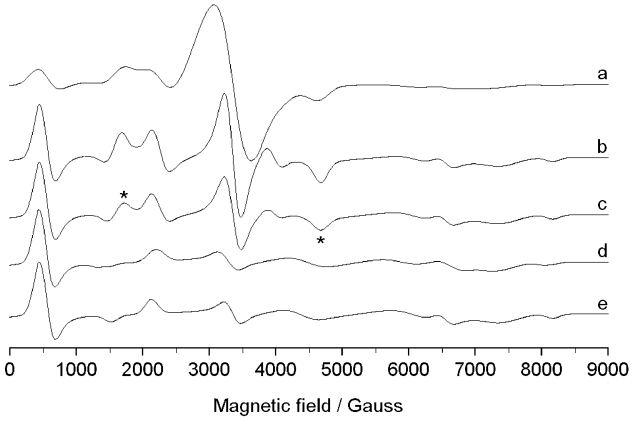

Figure 8. X-band EPR spectra recorded as a function of temperature on the polycrystalline powder of complex **1**: a) 60 K; b) 35 K; c) 20 K; d) 5 K and e) simulated spectrum of $S = 2$ spin state. The resonances attributable to the first excited $S = 1$ state are indicated with asterisk marks.

In order to assign the transitions between the spin states and to distinguish the spectra associated to each of them, the variation of the experimental spectra as a function of temperature must be examined. The series of X-band EPR spectra of complex **1** recorded between 0 and 9000 Gauss in the temperature range 5–60 K are shown in Figure 8. The spectra significantly change from 5 to 60 K exhibiting features extending from 0 to 8500 Gauss and it is evident that the transition around $g = 2$ gains intensity with the increase of temperature. In accordance with similar kind of $[CuL]_4$ complexes,[10,29,37] it can be proposed that below 10 K only the $S = 2$ spin state contributes to the experimental signal due to the high value of J. At higher temperatures, the three $S = 1$ states associated with the three values of J also become significantly populated and the observed spectrum originates from the participation of $S = 2$ as well as all the $S = 1$ states. However, since the energy splitting among the $S = 1$ levels are very different, the spectrum at 20 K and its comparison with those recorded at higher temperatures can give valuable information regarding the first excited $S = 1$ state. The resonances attributable to $S = 1$ state are indicated by asterisk marks in Figure 8 (c). If we assume that the separation between these transitions approximately corresponds to the zero-field splitting associated to $S = 1$ state and consider the rhombicity as negligible and g ca. 2, a value of $|D|$ ca. 0.3 cm^{-1} can be calculated.

At 20 K one can also detect the emergence of the broad transition centered around $g = 2$. At 60 K such a transition dominates the spectrum, which begins to resemble with the spectra both at liquid nitrogen and room temperature.

The spectrum recorded at 5 K was simulated (Figure 8, e) with the Hamiltonian in Equation (3).

$$\hat{H} = \beta \boldsymbol{H} \cdot \boldsymbol{g} \cdot \hat{\boldsymbol{S}} + \hat{\boldsymbol{S}} \cdot \boldsymbol{D} \cdot \hat{\boldsymbol{S}} \quad (3)$$

A good agreement with the experimental spectrum was obtained utilizing the following parameters: $g_x = g_y = 2.02$, $g_z = 2.10$, $|D| = 0.215\ cm^{-1}$ and $E/D = 0.088$. The D and E parameters are related to the tetragonal and rhombic distortion, respectively, and the ratio E/D can range between 0 for an axial symmetry and 0.333 in the limit of the maximum rhombic distortion. Therefore, our data are consistent with the structural features described above and eventually a symmetry corresponding to a slightly distorted axial system is represented. On the whole, the $S = 2$ spectrum of complex **1** is comparable to that of the recently reported tetranuclear Cu^{II} cubane complex formed by benzyl 2-deoxy-2-salicylideneamino-α-D-glucopyranoside, for which a D value of 0.246 cm^{-1} and E/D of 0.036 were measured.[29] This resemblance mainly arises from the similarity of J_1 values, 64.8 cm^{-1} for **1** and 64 cm^{-1} for the glucopyranoside derivative.

Catalytic Peroxidative Oxidation of Cyclohexane and Cycloheptane

We have studied the catalytic activity of the complex towards cyclohexane and cycloheptane oxidation using hydrogen peroxide as oxidant under the same experimental conditions for both the substrates. It is found that the tetranuclear copper(II) cluster acts as active catalyst for the liquid biphasic (acetonitrile/water) oxidation of cyclohexane and cycloheptane by H_2O_2 in a slightly acidic medium at room temperature and atmospheric pressure. Cyclic alcohols (i.e. cyclohexanol or cycloheptanol) and cyclic ketones (i.e. cyclohexanone or cycloheptanone) are obtained as the corresponding oxidized products. Optimization has been achieved by varying the relative proportions of nitric acid, hydrogen peroxide as well as time period of the reactions. In the literature,[38,39] it has been clearly pointed out that the presence of nitric acid has a positive role. It can activate the catalyst by promoting unsaturation at the metal center upon ligand protonation, with simultaneous increase in oxidation properties. As a result decomposition of peroxide is retarded and the peroxo intermediate gets stabilized.

Table 3. Peroxidative oxidation of cyclohexane and cycloheptane by complex **1**.

Entry	Catalyst	$n(H_2O_2)/n$(catalyst)	Time [h]	Yield (%)			TON[b]
				Cyclohexanol	Cyclohexanone	Total[a]	
1	complex **1**	150	6	19.2	16.0	35.2	13.0
2			48	26.3	19.6	45.9	17.0
3		300	6	28.1	15.4	43.5	16.1
4			48	32.3	19.5	51.8	19.2
5		750	6	21.6	15.2	36.8	13.6
6			48	29.0	17.3	46.3	17.2
7	$Cu(NO_3)_2$	150	48	1.8	1.1	2.9	–
8		300	48	3.4	1.7	5.1	–
9		750	48	3.6	1.8	5.4	–
Entry	Catalyst	$n(H_2O_2)/n$(catalyst)	Time [h]	Yield (%)			TON
				Cycloheptanol	Cycloheptanone	Total	
1	complex **1**	150	6	17.2	10.0	27.2	10.1
2			48	23.0	12.4	35.4	13.1
3		300	6	18.1	13.4	31.5	11.7
4			48	22.3	14.5	36.8	13.6
5		750	6	20.1	13.7	33.8	12.5
6			48	26.0	16.3	42.3	15.7
7	$Cu(NO_3)_2$	150	48	2.1	1.0	3.1	–
8		300	48	3.5	1.7	5.2	–
9		750	48	3.3	2.1	5.4	–

[a] Alcohol + ketone. [b] Turnover number (TON): moles of products divided by moles of catalyst.

During the present study, we have verified that the addition of nitric acid is mandatory in the hydrogen peroxide oxidation of cyclohexane and cycloheptane in presence of complex **1** as the catalyst. The amount of oxidized products remains almost unchanged in the 10–50 range of $n(HNO_3)/n$(catalyst), whereas further increase of such ratio decreases the yield. When the oxidation of the substrate was carried out in absence of nitric acid, the reaction did not proceed at all. The highest conversion of the substrate is achieved when $n(HNO_3)/n$(catalyst) is 10. The geometry around the Cu center in the catalyst is pentacoordinate having labile sites like Cu–μ_3-alkoxo-oxygen. These would require nitric acid so as to increase unsaturation at the metal site as a result of protonation of the NOO donor ligand. Such observations evoked us to maintain a ratio of $n(HNO_3)/n$(catalyst) = 10 in the rest of the studies.

The results of cyclohexane and cycloheptane oxidation are listed in Table 3. It is clearly seen from entries of the table that the product yields are highly influenced by the relative amounts of hydrogen peroxide, amount of nitric acid and the reaction period. The maximum overall yield of 51.8% was obtained for cyclohexane oxidation, when $n(H_2O_2)/n$(catalyst) ratio is 300 with the reaction time 48 h. Similarly, maximum conversions of cycloheptane to the corresponding cycloheptanol and cycloheptanone are 26.0 and 16.3%, respectively and turnover number (TON) up to 15.7 could be achieved at the higher peroxide-to-catalyst molar ratio of 750. The results of these oxidation reactions are comparable with those obtained for other copper complexes reported earlier.[25,38,40,41] In contrast, simple copper salt like, $Cu(NO_3)_2$ under the same reaction conditions exhibits a much lower activity towards oxidation of the substrates with 3.9–5.4% yield, under the same peroxide-to-catalyst molar ratio. Thus it is evident that the presence of N,O-ligands are quite relevant because such ligands can potentially be involved in proton-transfer steps.

In the case of complex **1**, the coordination environment around the copper(II) ion is easily accessible for an external ligand, as a result copper(II) can bind the peroxo group on treatment with peroxides. This in situ generated intermediate peroxo-type species seems to be capable of transferring the oxo-functionality to the organic substrates to give the corresponding oxidized products. In order to find out the probable mechanisms, we have carried out the catalytic reaction of cyclohexane with complex **1** maintaining $n(HNO_3)/n$(catalyst) ratio of 10 and $n(H_2O_2)/n$(catalyst) ratio of 300 in presence of TEMPO (2,2,6,6-tetramethylpiperidin-1-oxyl) and diphenylamine. The yield of the reaction is greatly suppressed in the presence of these compounds. TEMPO and diphenylamine are well known carbon-radical trap and oxygen-radical trap, respectively.[42] This indirectly indicates that oxidation reactions occur mainly by mechanisms involving the formation of both carbon-centered and oxygen-centered radicals. An organo-hydroperoxide intermediate of the type R-OOH (R = C_6H_{11}, C_7H_{13}) resulted from the reaction of a metal-peroxo intermediate, e.g. bearing a Cu^{II}–OOH type moiety, with the organo-radical R$^{\cdot}$ from the substrate can be proposed which has been reported for some other complexes also.[41,43] Thereby, final oxygenates are formed through H-abstraction or direct decomposition of the different free radicals e.g., alkoxyl (RO$^{\cdot}$) and alkylperoxyl (ROO$^{\cdot}$) generated from the homolytic decomposition of this organo-hydroperoxide intermediate. The proposed mechanistic pathway of the cycloalkane oxidation is summarized in Scheme 1.

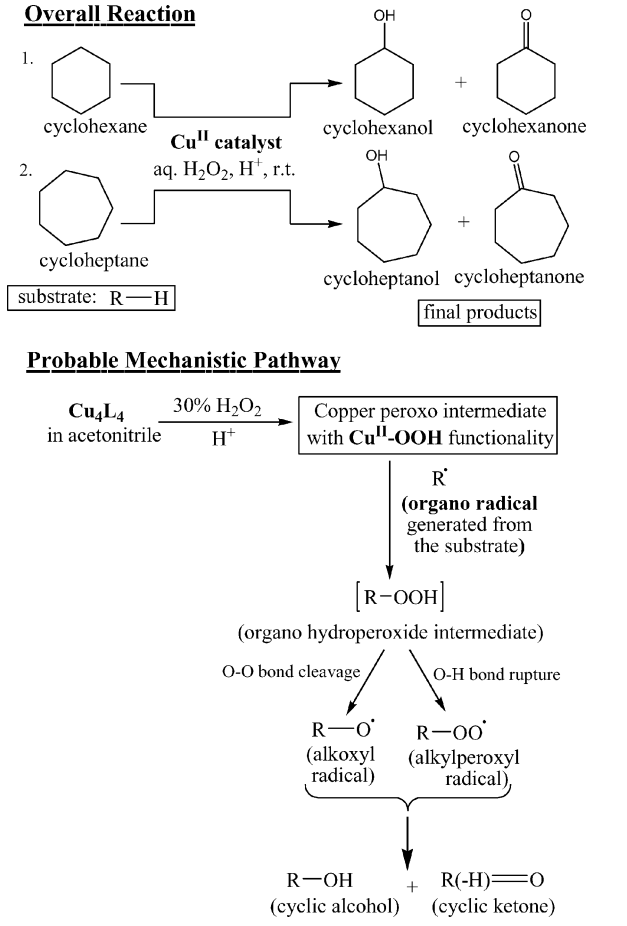

Scheme 1. Probable mechanistic pathway of catalytic oxidations of cycloalkanes.

Conclusions

In this paper, we presented a comprehensive discussion on the synthesis and structural characterizations of a new cubane-like Cu^{II} Schiff base complex. Variable-temperature magnetic susceptibility studies show that the tetranuclear copper cluster exhibits prominent intramolecular ferromagnetic spin exchange, associated with the close proximity of the copper centers and almost perpendicular arrangement of the adjacent Cu-magnetic orbitals ($d_{x^2-y^2}$) bearing the unpaired electrons. DFT calculations based on the X-ray crystal structure have been used to model the exchange process leading to the evaluation of the exchange coupling constants which are in conformity with the previous theoretical study on analogous complexes. The origin of two strong (J_1 and J_2) and a weak (J_3) ferromagnetic interaction can be explained by considering the distribution of long and short Cu–O bond lengths within each $\{Cu_2O_2\}$ face. The X-band EPR spectra recorded at low temperatures also confirm the ferromagnetic $S = 2$ ground state of **1**. Apart from the interesting magnetic properties, the complex is also found to possess efficient catalytic activities in the peroxidative oxidation of cyclohexane and cycloheptane which may proceed through an intermediate copper-peroxo species following radical mechanism. The corresponding cyclic alcohols and ketones are obtained in good amounts where total yields up to 52% can be achieved depending upon the reaction conditions.

Experimental Section

Physical Measurements: The Fourier transform infrared spectra of the ligand and the complex were recorded on a Perkin–Elmer Spectrum RX I FT-IR spectrophotometer with a KBr pressed pellet in the range 4000–200 cm^{-1}. The electronic spectra were recorded on a Perkin–Elmer Lambda 40 (UV/Vis) spectrometer using HPLC grade acetonitrile as solvent in the range 800–200 nm. Elemental analyses were carried out on a Perkin–Elmer 2400 II Elemental Analyser. Electron paramagnetic resonance (EPR) spectra of **1** were recorded on the polycrystalline powder with a X-band Varian E-9 or a Bruker EMX spectrometer at room temp. and LN temperature. For low temperature studies (5–35 K), an Oxford Instrument continuous-flow liquid helium cryostat and a temperature-control system were used. The spectra were simulated with the computer program Bruker WinEPR SimFonia.[44] Magnetic susceptibility measurements for the complex were carried out on polycrystalline sample with a Quantum Design SQUID MPMS-XL susceptometer apparatus working in the range 2–300 K under magnetic field of approximately 500 G (2–30 K) and 1000 G (35–300 K). Diamagnetic corrections were estimated from Pascal Tables. Gas chromatography analysis was performed with an Agilent Technologies 6890N network GC system equipped with a fused silica capillary column (30 mm × 0.32 mm) and a FID detector.

DFT Methodology and Computational Details: The exchange coupling constants in the tetranuclear Cu^{II} cubane studied in this paper have been calculated using the following computational methodology, described previously in the literature.[45,46] For the calculation of the exchange coupling constants for any polynuclear complex with n different exchange constants, at least the energy of $n + 1$ spin configurations must be calculated. In the case of the present tetranuclear complex, we have calculated the energy corresponding to eight different spin distributions to obtain by least-squares fitting the four exchange coupling constants with their standard deviations indicated in brackets. The eight spin distributions calculated correspond to the high spin solution, one $S = 2$: [+,+,+,+], four $S = 1$: [–,+,+,+], [+,–,+,+], [+,+,–,+], [+,+,+,–] and three $S = 0$: [+,+,–,–], [+,–,–,+], [+,–,+,–]. The hybrid B3LYP functional[47] has been used in all calculations as implemented in Gaussian 03.[48] The guess functions were generated with Jaguar 6.0.[49] Basis sets proposed by Schaefer et al.[50] have been employed throughout: a triple-ξ all electron basis set with two p polarization function for copper atoms[51] and a double-ξ all electron for the other elements. All energy calculations were performed including 10^{-8} density-based convergence criterion.

Materials: 5-chlorosalicylaldehyde and ethanolamine were purchased from Sigma Aldrich, USA. Copper(II) perchlorate hexahydrate was prepared by the treatment of basic copper(II) carbonate, $CuCO_3{\cdot}Cu(OH)_2$ (E. Merck, India) with 80% perchloric acid (E. Merck, India) followed by slow evaporation on a steam bath. It was then filtered through a fine glass-frit and preserved in $CaCl_2$ desiccator. All the chemicals and solvents employed for the syntheses were of analytical grade and used as received without further purification. Cyclohexane, cycloheptane, cyclohexanone, cyclohexanol, cycloheptanone, cycloheptanol, cyclopentanone were purchased from Sigma Aldrich, USA and used as received. Solvents

used for spectroscopic studies were purified and dried by standard procedures before use.[52]

Caution! *Perchlorate salts are potentially explosive in the presence of organic materials. They should be prepared in small amounts and handled with extreme care.*

Synthesis of the Schiff Base Ligand (H_2L): Ethanolamine (0.12 mL, 2 mmol) was added to a solution of 5-chlorosalicylaldehyde (0.313 g, 2 mmol) in 20 mL methanol and the mixture was refluxed for 1 h at 65 °C. Then a deep yellow solution was obtained which upon cooling yielded yellow crystalline solid as the ligand. The product was collected by filtration, washed with diethyl ether and dried at room temperature. Yield 0.170 g (85%). $C_9H_{10}ClNO_2$ (199.63): calcd. C 54.15, H 5.05, N 7.02; found C 54.17, H 5.02, N 7.04. FT-IR (KBr, cm^{-1}): ν(C=N) 1640 cm^{-1}. UV/Vis (λ, nm): 261, 393.

Synthesis of $[Cu_4L_4]\cdot 2H_2O$ (1): The appropriate quantity of solid Schiff base ligand H_2L (0.199 g, 1 mmol) was dissolved in 20 mL of methanol. This ligand solution was added dropwise to a 10 mL methanolic solution of $Cu(ClO_4)_2\cdot 6H_2O$ (0.370 g, 1 mmol) with constant stirring. The mixture was refluxed for 45 min at 60 °C. The resulting deep green solution was then filtered and the filtrate was left undisturbed. After 5 d green plate shaped X-ray diffraction quality single crystals appeared. Yield 0.886 g (82%). $C_{36}H_{36}Cl_4Cu_4N_4O_{10}$ (1080.69): calcd. C 40.01, H 3.36, N 5.18; found C 40.04, H 3.32, N 5.15.

Experimental Procedure for Catalytic Studies: The catalytic hydrocarbon oxidation reactions by complex **1** involving cyclohexane and cycloheptane as substrates were carried out with the following procedure: 2.5–10.0 mmol of hydrogen peroxide (30% in H_2O) was added to the metal complex (0.025 mmol) in 3 mL of acetonitrile in a two-neck round-bottomed flask fitted with a condenser. To this solution, HNO_3 (0.250 mmol) was added followed by the addition of 0.927 mmol of substrate. The reaction was initiated by stirring the above mixture for 48 h at room temperature under atmospheric pressure. Aliquots were collected after regular time intervals and 90 μL of cyclopentanone was added as internal standard. The substrate and products from the reaction mixture were extracted with 10 mL of diethyl ether and they were analyzed by gas chromatography. The identification was achieved by comparison with known standards.

X-ray Crystallographic Study: A diffraction-quality single-crystal of **1** was mounted on an Oxford Diffraction Gemini-R diffractometer equipped with a graphite monochromator and Cu-K_α radiation (λ = 1.5418 Å). The crystallographic data collection was performed using multi scan technique at 200 K. Data collection and the unit cell refinement were performed using CrysAlisPRO software.[53] The structure of the complex was solved by direct method procedures with SHELXS,[54a] and refined by full-matrix least-squares based on F^2 with SHELXL.[54b] The non-hydrogen atoms were refined with anisotropic factors. All hydrogen atoms were positioned geometrically treated as riding on the bound atom and those of the water molecules were located in difference Fourier maps. All of the crystallographic computations and graphical works were carried out using PLATON99[55] and ORTEP[56] programs. A summary of the crystallographic data and details of the structure refinements are listed in Table 4.

CCDC-727916 (for **1**) contains the supplementary crystallographic data for this paper. These data can be obtained free of charge from The Cambridge Crystallographic Data Centre via www.ccdc.cam.ac.uk/data_request/cif.

Table 4. Crystallographic data and refinement parameters for **1**.

Empirical formula	$C_{36}H_{36}Cl_4Cu_4N_4O_{10}$
Formula weight	1080.69
Crystal dimension [mm]	$0.1242 \times 0.1087 \times 0.0215$
Crystal system	orthorhombic
Space group	*Pbcn*
a [Å]	19.0796(5)
b [Å]	22.1237(7)
c [Å]	9.3677(4)
V [Å^3]	3954.2(2)
Z	4
T [K]	200(2)
$\lambda_{Cu\text{-}K\alpha}$ [Å]	1.5418
D_c [g cm^{-3}]	1.815
μ [mm^{-1}]	5.446
F(000)	2176
θ [°]	4.00 to 73.78
Total data	21296
Unique data	3891
Observed data [$I > 2\sigma(I)$]	2225
R[a]	0.0554
R_w[b]	0.1208
Goodness-of-fit on F^2, S	0.925
R_{int}	0.0926
$\Delta\rho_{max}$ [e Å^{-3}]	0.531
$\Delta\rho_{min}$ [e Å^{-3}]	–0.481

[a] $R = \Sigma(|F_o - F_c|)/\Sigma|F_o|$. [b] $R_w = \{\Sigma[w(|F_o - F_c|)^2]/\Sigma[w|F_o|^2]\}^{0.5}$.

Acknowledgments

S. T. gratefully acknowledges the Indian Council of Scientific and Industrial Research (CSIR), New Delhi for the award of a Senior Research Fellowship to her [CSIR Sanction No.09/096(0519)/2007-EMR-I]. Thanks are extended to Prof. P. Banerjee of the Department of Inorganic Chemistry, Indian Association for the Cultivation of Science, Kolkata-32 for help with the catalytic studies. The authors are also thankful to the All India Council for Technical Education for financial support. The authors are also grateful for the financial support given by the Spanish government (CTQ2006-01759/BQU, CTQ2005-08123-C02-02/BQU) and the Catalan government (2005SGR-00593, 2005SGR-00036). J. T. is grateful to the Centre de Computació de Catalunya (CESCA) for a grant provided by Fundació Catalana per a la Recerca (FCR) and the Universitat de Barcelona.

[1] a) F. De Angelis, S. Fantacci, A. Sgamellotti, E. Cariati, R. Ugo, P. C. Ford, *Inorg. Chem.* **2006**, *45*, 10576–10584; b) C. Mukherjee, T. Weyhermüller, E. Bothe, E. Rentschler, P. Chaudhuri, *Inorg. Chem.* **2007**, *46*, 9895–9905.
[2] B. F. Abrahams, S. J. Egan, R. Robson, *J. Am. Chem. Soc.* **1999**, *121*, 3535–3536.
[3] A. Mukherjee, M. Nethaji, A. R. Chakravarty, *Angew. Chem. Int. Ed.* **2004**, *43*, 87–90.
[4] a) J. Sun, C. Tessier, R. H. Holm, *Inorg. Chem.* **2007**, *46*, 2691–2699; b) P. Zanello, *Coord. Chem. Rev.* **1988**, *83*, 199–275.
[5] S. M. Malinak, A. M. Simeonov, P. E. Mosier, C. E. McKenna, D. Coucouvanis, *J. Am. Chem. Soc.* **1997**, *119*, 1662–1667.
[6] a) A. T. Fiedler, T. C. Brunold, *Inorg. Chem.* **2005**, *44*, 9322–9334; b) R. H. Holm, S. Ciurli, J. A. Weigel, *Progress in Inorganic Chemistry: Bioinorganic Chemistry*, New York, **1990**, *38*, p. 1.

[7] a) J. Sletten, A. Sørensen, M. Julve, Y. Journaux, *Inorg. Chem.* **1990**, *29*, 5054–5058; b) J. A. Real, G. De Munno, R. Chiappetta, M. Julve, F. Lloret, Y. Journaux, J.-C. Colin, G. Blondin, *Angew. Chem. Int. Ed. Engl.* **1994**, *33*, 1184–1186.

[8] a) X. S. Tan, Y. Fujii, R. Nukada, M. Mikuriya, Y. Nakano, *J. Chem. Soc., Dalton Trans.* **1999**, 2415–2416; b) L. P. Wu, T. Kuroda-Sowa, M. Maekawa, Y. Suenaga, M. Munakata, *J. Chem. Soc., Dalton Trans.* **1996**, 2179–2180.

[9] a) H. Oshio, Y. Saito, T. Ito, *Angew. Chem. Int. Ed. Engl.* **1997**, *36*, 2673–2675; b) J. K. Eberhardt, T. Glaser, R.-D. Hoffmann, R. Fröhlich, E. U. Würthwein, *Eur. J. Inorg. Chem.* **2005**, 1175–1181.

[10] C. Aronica, Y. Chumakov, E. Jeanneau, D. Luneau, P. Neugebauer, A.-L. Barra, B. Gillon, A. Goujon, A. Cousson, J. Tercero, E. Ruiz, *Chem. Eur. J.* **2008**, *14*, 9540–9548.

[11] a) N. Lopez, T. E. Vos, A. M. Arif, W. W. Shum, J. C. Noveron, J. S. Miller, *Inorg. Chem.* **2006**, *45*, 4325–4327; b) R. Wegner, M. Gottschaldt, H. Görls, E.-G. Jäger, D. Klemm, *Chem. Eur. J.* **2001**, *7*, 2143–2157.

[12] a) O. Kahn, *Molecular Magnetism*, VCH Publishers: New York, **1993**; b) J. H. Rodriguez, J. K. McCusker, *J. Chem. Phys.* **2002**, *116*, 6253–6270.

[13] E. Ruiz, A. Rodríguez-Fortea, J. Tercero, T. Cauchy, *J. Chem. Phys.* **2005**, *123*, 074102/1–10.

[14] M. Fondo, A. M. García-Deibe, M. Corbella, E. Ruiz, J. Tercero, J. Sanmartín, M. R. Bermejo, *Inorg. Chem.* **2005**, *44*, 5011–5020.

[15] a) E. Ruiz, P. Alemany, S. Alvarez, J. Cano, *J. Am. Chem. Soc.* **1997**, *119*, 1297–1303; b) E. Ruiz, P. Alemany, S. Alvarez, J. Cano, *Inorg. Chem.* **1997**, *36*, 3683–3688.

[16] a) E. I. Solomon, U. M. Sundaram, T. E. Machonkin, *Chem. Rev.* **1996**, *96*, 2563–2606; b) W. Kaim, J. Rall, *Angew. Chem. Int. Ed. Engl.* **1996**, *35*, 43–60.

[17] a) A. P. Cole, D. E. Root, P. Mukherjee, E. I. Solomon, T. D. P. Stack, *Science* **1996**, *273*, 1848–1850; b) P. Roy, K. Dhara, M. Manassero, P. Banerjee, *Inorg. Chem. Commun.* **2008**, *11*, 265–269.

[18] a) S. J. Elliot, M. Zhu, L. Tso, H.-H. T. Nguyen, J. H.-K. Yip, S. I. Chan, *J. Am. Chem. Soc.* **1997**, *119*, 9949–9955; b) J. Yoon, E. I. Solomon, *Inorg. Chem.* **2005**, *44*, 8076–8086.

[19] a) R. Whyman, *Applied Organometallic Chemistry and Catalysis*, Oxford University Press, Oxford, **2001**; b) A. E. Shilov, G. B. Shul′pin, *Activation and Catalytic Reactions of Saturated Hydrocarbons in the Presence of Metal Complexes*, Kluwer Academic Publishers, Dordrecht, The Netherlands, **2000**.

[20] a) M. C. Mimmi, M. Gullotti, L. Santagostini, G. Battaini, E. Monzani, R. Pagliarin, G. Zoppellaro, L. Casella, *Dalton Trans.* **2004**, 2192–2201; b) L. M. Mirica, X. Ottenwaelder, T. D. P. Stack, *Chem. Rev.* **2004**, *104*, 1013–1046; c) E. A. Lewis, W. B. Tolman, *Chem. Rev.* **2004**, *104*, 1047–1076.

[21] C. R. Choudhury, S. K. Dey, R. Karmakar, C.-D. Wu, C.-Z. Lu, M. S. El Fallah, S. Mitra, *New J. Chem.* **2003**, *27*, 1360–1366.

[22] a) P. Talukder, S. Sen, S. Mitra, L. Dahlenberg, C. Desplanches, J.-P. Sutter, *Eur. J. Inorg. Chem.* **2006**, 329–333; b) A. Datta, C. R. Choudhury, P. Talukder, S. Mitra, L. Dahlenburg, T. Matsushita, *J. Chem. Res. (S)* **2003**, 642–644.

[23] a) S. Thakurta, J. Chakraborty, G. Rosair, J. Tercero, M. S. El Fallah, E. Garribba, S. Mitra, *Inorg. Chem.* **2008**, *47*, 6227–6335; b) J. Chakraborty, S. Thakurta, G. Pilet, D. Luneau, S. Mitra, *Polyhedron* **2009**, *28*, 819–825.

[24] K. Nakamoto, *Infrared and Raman Spectra of Inorganic and Coordination Compounds*, 5th ed., John Wiley, New York, **1997**.

[25] S. Thakurta, P. Roy, G. Rosair, C. J. Gómez-García, E. Garribba, S. Mitra, *Polyhedron* **2009**, *28*, 695–702.

[26] Z.-L. You, H.-L. Zhu, *Z. Anorg. Allg. Chem.* **2004**, *630*, 2754–2760.

[27] A. B. P. Lever, *Inorganic Electronic Spectroscopy*, 2nd ed., Elsevier, Amsterdam, **1984**.

[28] A. W. Addison, T. N. Rao, J. Reedijk, J. van Rijn, G. C. Verschoor, *J. Chem. Soc., Dalton Trans.* **1984**, 1349–1356.

[29] A. Burkhardt, E. T. Spielberg, H. Görls, W. Plass, *Inorg. Chem.* **2008**, *47*, 2485–2493.

[30] J. Tercero, E. Ruiz, S. Alvarez, A. Rodríguez-Fortea, P. Alemany, *J. Mater. Chem.* **2006**, *16*, 2729–2735 and references cited therein.

[31] J. W. Hall, W. E. Estes, E. D. Estes, R. P. Scaringe, W. E. Hatfield, *Inorg. Chem.* **1977**, *16*, 1572–1574.

[32] J. Cano, E. Ruiz, S. Alvarez, M. Verdaguer, *Comments Inorg. Chem.* **1998**, *20*, 27–56.

[33] T. Shimada, M. Kodera, H. Okawa, S. Kida, *J. Chem. Soc., Dalton Trans.* **1992**, 1121–1125.

[34] M. Insausti, L. Lezama, R. Cortes, I. Gil de Muro, T. Rojo, M. I. Arriortua, *Solid State Commun.* **1995**, *93*, 823–828.

[35] N. Gouskos, V. Likodimos, C. A. Londos, V. Psycharis, C. Mitros, A. Koufoudakis, H. Gamari-Seale, W. Windsch, H. Metz, *J. Solid State Chem.* **1995**, *119*, 50–61.

[36] F. Nepveu, *Inorg. Chim. Acta* **1987**, *134*, 43–48.

[37] N. Matsumoto, T. Kondo, M. Kodera, H. Okawa, S. Kida, *Bull. Chem. Soc. Jpn.* **1989**, *62*, 4041–4043.

[38] A. M. Kirillov, M. N. Kopylovich, M. V. Kirillova, M. Haukka, M. F. C. Guedes da Silva, A. J. L. Pombeiro, *Angew. Chem. Int. Ed.* **2005**, *44*, 4345–4349.

[39] P. Roy, K. Dhara, M. Manassero, P. Banerjee, *Eur. J. Inorg. Chem.* **2008**, 4404–4412.

[40] A. M. Kirillov, M. N. Kopylovich, M. V. Kirillova, E. Yu. Karabach, M. Haukka, M. F. C. Guedes da Silva, A. J. L. Pombeiro, *Adv. Synth. Catal.* **2006**, *348*, 159–174.

[41] C. D. Nicola, E. Yu. Karabach, A. M. Kirillov, M. Monari, L. Pandolfo, C. Pettinari, A. J. L. Pombeiro, *Inorg. Chem.* **2007**, *46*, 221–230.

[42] L. M. Slaughter, J. P. Collman, T. A. Eberspacher, J. I. Brauman, *Inorg. Chem.* **2004**, *43*, 5198–5204.

[43] M. Costas, M. P. Mehn, M. P. Jensen, L. Que Jr., *Chem. Rev.* **2004**, *104*, 939–986.

[44] Bruker Analytische Messtechnik GmbH, *WINEPR SimFonia*, version 1.25, Karlsruhe, Germany, **1996**.

[45] J. Cano, R. Costa, S. Alvarez, E. Ruiz, *J. Chem. Theory Comput.* **2007**, *3*, 782–788.

[46] E. Ruiz, *Struct. Bonding (Berlin)* **2004**, *113*, 71–102.

[47] A. D. Becke, *J. Chem. Phys.* **1993**, *98*, 5648–5652.

[48] M. J. Frisch, G. W. Trucks, H. B. Schlegel, G. E. Scuseria, M. A. Robb, J. R. Cheeseman, J. A. Montgomery, T. Vreven, K. N. Kudin, J. C. Burant, J. M. Millam, S. S. Iyengar, J. Tomasi, V. Barone, B. Mennucci, M. Cossi, G. Scalmani, N. Rega, G. A. Petersson, H. Nakatsuji, M. Hada, M. Ehara, K. Toyota, R. Fukuda, J. Hasegawa, H. Ishida, T. Nakajima, Y. Honda, O. Kitao, H. Nakai, M. Klene, X. Li, J. E. Knox, H. P. Hratchian, J. B. Cross, C. Adamo, J. Jaramillo, R. Gomperts, R. E. Stratmann, O. Yazyev, A. J. Austin, R. Cammi, C. Pomelli, J. Ochterski, P. Y. Ayala, K. Morokuma, G. A. Voth, P. Salvador, J. J. Dannenberg, V. G. Zakrzewski, S. Dapprich, A. D. Daniels, M. C. Strain, O. Farkas, D. K. Malick, A. D. Rabuck, K. Raghavachari, J. B. Foresman, J. V. Ortiz, Q. Cui, A. G. Baboul, S. Clifford, J. Cioslowski, B. B. Stefanov, G. Liu, A. Liashenko, P. Piskorz, I. Komaromi, R. L. Martin, D. J. Fox, T. Keith, M. A. Al-Laham, C. Y. Peng, A. Nanayakkara, M. Challacombe, P. M. W. Gill, B. Johnson, W. Chen, M. W. Wong, C. Gonzalez, J. A. Pople, *Gaussian 03 (Revision B.4)*, Pittsburgh, PA, **2003**.

[49] Schrodinger Inc., *Jaguar 6.0*, Portland, **2005**.

[50] A. Schaefer, H. Horn, R. Ahlrichs, *J. Chem. Phys.* **1992**, *97*, 2571–2577.

[51] A. Schaefer, C. Huber, R. Ahlrichs, *J. Chem. Phys.* **1994**, *100*, 5829–5835.

[52] D. D. Perrin, W. L. F. Armarego, D. R. Perrin, *Purification of Laboratory Chemicals*, 2nd ed., Pergamon Press, Oxford, UK, **1980**.

[53] Oxford Diffraction Ltd., Crysalis Software system, *CrysAlis PRO*, Abingdon, UK, **2007**.
[54] a) G. M. Sheldrick, *SHELXS-97, Program for crystal structure determination*, University of Göttingen, Germany, **1997**; b) G. M. Sheldrick, *SHELXL-97, Program for crystal structure refinement*, University of Göttingen, Germany, **1997**.
[55] A. L. Spek, *PLATON, Molecular Geometry Program*, University of Utrecht, The Netherlands, **1999**.
[56] L. J. Farrugia, *ORTEP3 for Windows*, *J. Appl. Crystallogr.* **1997**, *30*, 565.

Received: June 2, 2009
Published Online: September 3, 2009

